Brownian flocculation of polymer colloids in the presence of a secondary minimum

William R. Schowalter* and Alec B. Eidsath†

Department of Chemical Engineering, University of Illinois, Urbana, IL 61801

Contributed by William R. Schowalter, January 16, 2001

This contribution is part of the special series of Inaugural Articles by members of the National Academy of Sciences elected on April 28, 1998.

Most analyses of Brownian flocculation apply to conditions where London–van der Waals attractive forces cause particles to be strongly bound in a deep interparticle potential well. In this paper, results are reported that show the interaction between primary- and secondary-minimum flocculation when the interparticle potential curve reflects both attractive and electrostatic repulsive forces. The process is highly time-dependent because of transfer of particles from secondary- to primary-minimum flocculation. Essential features of the analysis are corroborated by experiments with 0.80-μm polystyrene spheres suspended in aqueous solutions of NaCl over a range of ionic strengths. In all cases, experiments were restricted to the initial stage of coagulation, where singlets and doublets predominate.

Factors governing the tendency of colloidal particles to flocculate into multiparticle aggregates or to remain dispersed are central to numerous commercial applications ranging from water purification to cosmetics. The first quantitative analyses of coagulation kinetics were performed by von Smoluchowski (1), and his results continue to influence both the nomenclature and theoretical approaches to the subject. For a general review, the reader is referred to Russel, *et al.* (2).

The mechanics of coagulation are conveniently divided into "rapid" and "slow" regimes, a stable dispersion being an extreme of the "slow" coagulation category. In the case of lyophobic colloids with near-spherical geometry, the distinction between the two regimes is readily associated with the nature of the interparticle potential curve. To an approximation that has proved remarkably robust, the Derjaguin, Verwey, Landau, and Overbeek (DLVO) theory of the 1940s (2) incorporates the essential physics for a colloid dispersed in an ionic medium. Coagulation is favored by a London–van der Waals attractive force that is characterized by a potential with an h^{-1} and an h^{-6} dependence at small and large particle separations, respectively, where h is the gap between particle surfaces. However, ions present on a particle surface give rise to a shell of counterions in the liquid surrounding each particle. The result is an electrostatic repulsion between particles that favors slow coagulation, or stability.

When London–van der Waals attractive forces are dominant, the initial stage of coagulation (called here flocculation to indicate that only coagulation of single particles to form doublets is being considered) is reasonably well understood (3–5). Dominant attractive forces can occur when the electrostatic potential at a particle surface and the ionic strength of the dispersing medium are sufficiently high to ensure an electrical double layer around each particle that is thin relative to the particle size. Then the interparticle potential curve is everywhere attractive, up to extremely small separations, where strong repulsive forces (Born repulsion) dominate. Thus, the particles are tightly bound in a primary minimum potential well. As the ionic strength of the dispersing medium is reduced, the double layer expands and, if the particle surface potential is sufficiently high, the interparticle potential curve can exhibit both a primary and secondary minimum (Fig. 1). When the potential barrier between primary and secondary minima is sufficiently high, the coagulation process becomes "slow" and in an extreme the dispersion is judged to be "stable."

In this work, we address the kinetics of flocculation under conditions where flocculation into the secondary minimum (shown in Fig. 1) is important. We shall show that secondary- and primary-minimum flocculations are generally interrelated, and that it is necessary to consider the time-dependent nature of the flocculation process. The analysis and experiments described here are restricted to flocculation from encounters due to Brownian motion. Good agreement between theoretical prediction and experiments is found for the dependence of flocculation behavior on changes in electrolyte concentration of the dispersing medium. However, there is an offset between the numerical values predicted and observed. This offset may be due to an insufficiently complete description of interparticle forces.

Feke and Prabhu (6) used a series expansion method to model secondary minimum flocculation. A steady state Boltzmann distribution of particles was subjected to a change in ionic strength and the redistribution of particles was followed. Because of the parameters chosen in their study, which included a barrier of nearly 100kT between primary and secondary minima, significant flocculation into the primary minimum is unlikely.

In the work presented here, we account for the series nature of flocculation, in which particles attracted into a secondary minimum can subsequently proceed into a primary minimum. Flocculation into the secondary minimum is time-dependent because of the limited depth of that minimum. Eventually, one reaches an equilibrium concentration in the secondary minimum, even though aggregation continues in the primary minimum.

Theory of Brownian Coagulation

Problem Formulation. We begin with a conservation equation for the pair distribution function $P(\mathbf{r},t)$, the probability that, given a particle at the origin at time t, there will be a particle in an element of volume $d\mathbf{r}$ centered around $\mathbf{r}$. The probability function $P(\mathbf{r},t)$ can be expressed as a relative probability by suitable normalization. Following page 488 of ref. 2, and equating particle mobility to $\mathbf{D}/kT$, one can write

$$\frac{\partial P}{\partial t} + \nabla\cdot[(\mathbf{U} + (\mathbf{D}/kT)\cdot\mathbf{F})P] = \nabla\cdot(\mathbf{D}\cdot\nabla P), \qquad [1]$$

where $\mathbf{U}$ = bulk velocity, $\mathbf{D}$ = particle diffusivity, k = Boltzmann's constant, and T = temperature. The interparticle force is assumed to be spherically symmetric and derivable from a potential V_T,

$$\mathbf{F} = -\nabla V_T \qquad [2]$$

Because we are considering only Brownian effects in a system with no bulk flow, $\mathbf{U} \equiv \mathbf{0}$. Eq. **1** can be rewritten in dimensionless

*To whom reprint requests should be addressed at: 306 Engineering Hall, MC-266, 1308 West Green Street, Urbana, IL 61801. E-mail: schow@uiuc.edu.

†Present address: Division of Bioengineering and Physical Science, ORS/OD/National Institutes of Health, Building 13, Room 3N18, Bethesda, MD 20892-5766.

 www.pnas.org/cgi/doi/10.1073/pnas.061028498

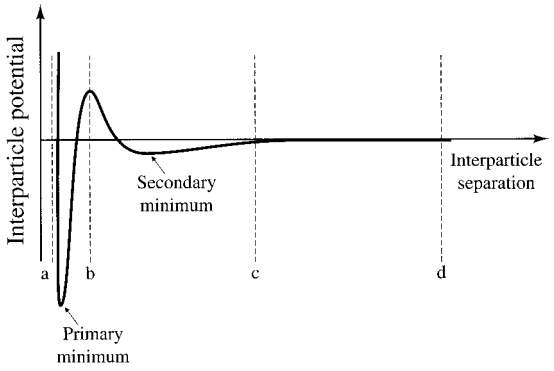

Fig. 1. Schematic representation of interparticle potential showing regions of interest.

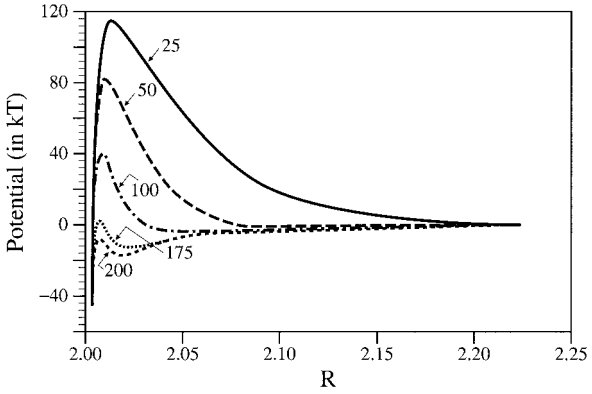

Fig. 3. Interparticle potentials for five values of $a\kappa$, by using physical parameters from ref. 6.

form with the scaling $R = r/a$, $\tau = t/t_0$, $\mathbf{D}^* = \mathbf{D}/D_0$, $V = V_T/kT$, $t_0 = 3\pi\mu a^3/\kappa T$, and $D_0 = kT/3\pi\mu a$, where a = particle radius (assuming spherical particles) and μ = fluid viscosity. Then

$$\frac{\partial P}{\partial t} = \nabla\cdot[\mathbf{D}^*\cdot(P\nabla V + \nabla P)]. \qquad [3]$$

We wish to solve Eq. **3** subject to boundary conditions that specify no particle flux at $R = 2$ (the particles cannot interpenetrate), and $P = 1$ as $R \to \infty$, meaning that the far field distribution is homogeneous and replenished as particles leave the singlet state through flocculation with a test particle centered at $R = 0$. These conditions are close to those realized experimentally during the initial stages of aggregation, over which there is little change in the singlet particle concentration. An initial condition is chosen to match a situation where a homogeneous, nonaggregated suspension is subjected to an increase in electrolyte concentration, whereupon flocculation begins. To ensure initial aggregation in a secondary minimum we impose the condition $P(t = 0) = 0$ in a small region very near to $R = 1$.

Interparticle colloidal forces are modeled by the conventional DLVO theory,

$$V = V_A + V_R + V_B. \qquad [4]$$

The attractive potential is given by

$$V_A = -\frac{A_{eff}}{6kT}\left[\frac{2}{R^2-4} + \frac{2}{R^2} + \ln\left(\frac{R^2-4}{R^2}\right)\right], \qquad [5]$$

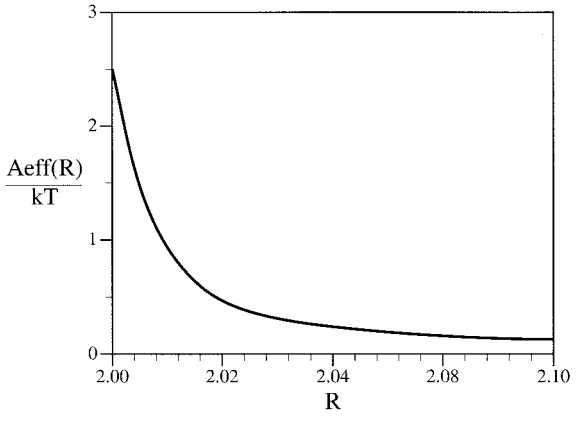

Fig. 2. Effective Hamaker coefficient according to Lifshitz theory (2).

where the Lifshitz theory is used to estimate the Hamaker function A_{eff}. For details, the reader is referred to Russel, *et al.* (2) and Eidsath (7). A plot of $A_{eff}(R)/kT$ as a function of separation is shown in Fig. 2.

A reasonable approximation of the repulsive potential for $e\psi_0/kT < 2$ is

$$V_R = \frac{2\pi\varepsilon\psi_0^2 a}{kT}\ln[1 + \exp(-a\kappa(R-2))], \qquad [6]$$

where ε = dielectric constant, κ = the inverse Debye length ($a\kappa$ is a dimensionless quantity describing the inverse double layer thickness), ψ_0 = surface potential, and e = charge on an electron. Surface potentials were inferred from electrophoretic measurements of zeta potential, ζ_0, and assuming $\zeta_0 = e\psi_0/kT$.

Finally, for the Born repulsion we use (8)

$$V_B = \frac{C_B}{R}\left[\frac{R^2-14R+54}{(R-2)^7} + \frac{-2R^2+60}{R^7} + \frac{R^2+14R+54}{(R+2)^7}\right]. \qquad [7]$$

We have taken $C_B = 1.0 \times 10^{-22}$. This value for C_B results in a primary minimum of approximately 600 kT. The location of the primary minimum is $R \cong 2.0005$ and it varies by approximately 0.0002 for a change in C_B of one decade. For a typical case, the potential is zero at $R = 2.0004$, -600 kT at $R = 2.00055$ and at the primary maximum at $R = 2.006$. The far-field boundary

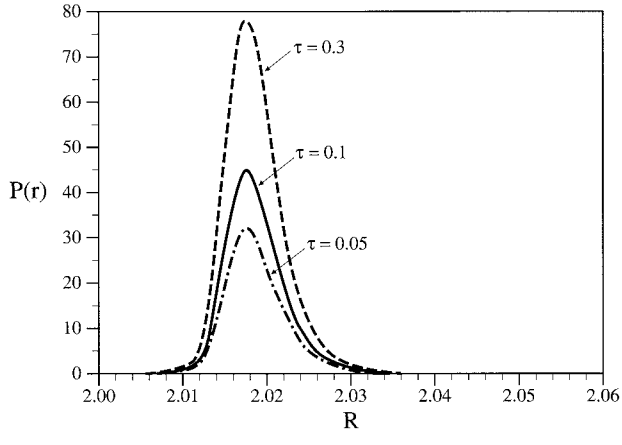

Fig. 4. Filling of the secondary-minimum well for short times. $a\kappa = 200$ and the characteristic time is 35 s.

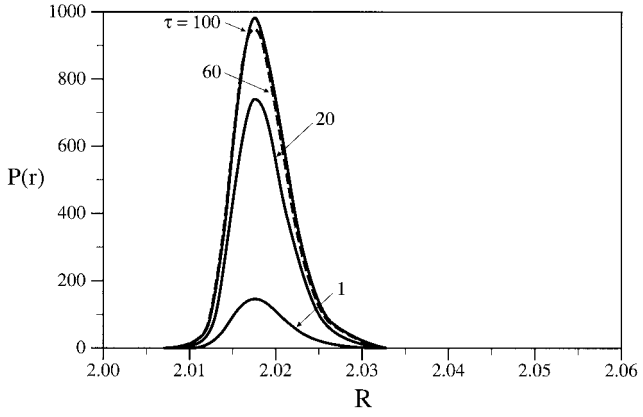

Fig. 5. The long-time pair distribution function, showing the approach to equilibrium for $a\kappa = 200$.

condition was invoked at $R \cong 5$. These scales can be applied to the schematic diagram of Fig. 1.

Because we are considering a system in which there is no bulk flow, all hydrodynamic effects are exhibited in the Brownian diffusion coefficient **D**. Because of the spherical symmetry of the problem, the hydrodynamics are expressed in terms of the known function G(R) (9). Then Eq. **3** becomes the scalar equation

$$\frac{\partial P}{\partial \tau} = \frac{1}{R^2}\frac{\partial}{\partial R}\left\{R^2 G(R)\left[\frac{\partial P}{\partial R} + P\frac{\partial V}{\partial R}\right]\right\}, \qquad [8]$$

where

$$\mathbf{D}(\mathbf{r}) = \frac{kT}{3\pi\mu a} G(r)\frac{\mathbf{rr}}{r^2}.$$

Boundary conditions for the solution of Eq. **8** are: the no-flux condition as particles approach each other,

$$G(R)\left\{\frac{\partial P}{\partial R} + P\frac{\partial V}{\partial R}\right\} = 0 \text{ as } R \to 2, \qquad [9a]$$

and uniform concentration as one approaches a large distance from the test particle,

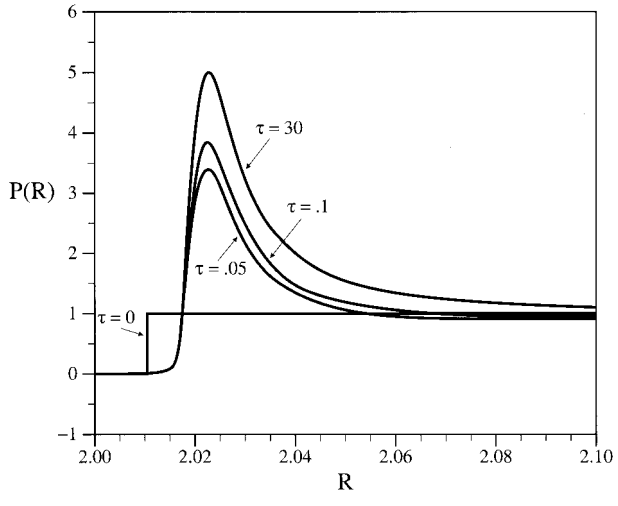

Fig. 6. The pair distribution function for colloidal parameters used in experiments ($a\kappa = 346$, $\zeta_0 = 2.06$, [NaCl] = 0.07 M). The characteristic time is 0.15 s.

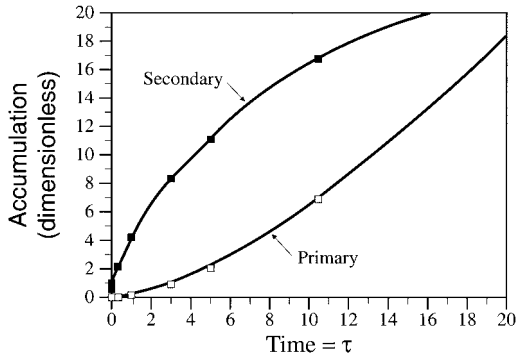

Fig. 7. Accumulation at short times for $a\kappa = 200$.

$$P = 1 \text{ as } R \to \infty. \qquad [9b]$$

As noted earlier, the initial condition is $P = 1$ at $t = 0$ for all space except for a thin shell around the test sphere, for which $P = 0$.

Referring to Fig. 1, it is clear that, knowing P(r,t), the dimensionless net accumulation of particles between two shells 1 and 2 can be computed (to within a numerical constant) for a time interval $\bar{\tau}$ by

$$\int_0^{\bar{\tau}}\left\{R^2 G(R)\left[\frac{\partial P}{\partial R} + P\frac{\partial V}{\partial R}\right]\right\}_1^2 d\tau. \qquad [10]$$

By identifying shells 1 and 2 with a, b, and c of Fig. 1, respectively, one can compute primary, secondary, or total aggregation over the interval. (Note that in the experiments, only total aggregation is measured.)

Method of Solution. Because the primary minimum was always very deep [O(600 kT)], the flux across b is independent of the concentration of particles in the primary minimum; hence it was not necessary to solve for the pair distribution function in the entire domain, and we need to find P(r,t) only in the region between b and d in Fig. 1. Furthermore, because of the deep primary minimum we can simplify the boundary conditions to

$$P = 0 \text{ at } R = R_{pm}, \text{ and } P = 1 \text{ as } R \to \infty, \qquad [11]$$

where R_{pm} refers to the location of the primary maximum.

Eq. **8** was solved with implicit time stepping and three-point central differences. The spatial domain was described by $X = \sqrt{R-2}$, which allowed closer placement of nodes where they were needed. Alternate numerical techniques (7) did not have an important effect on results. For the most part, the outer bound-

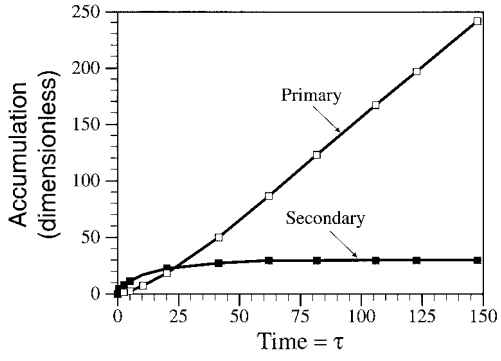

Fig. 8. Accumulation at long times for $a\kappa = 200$.

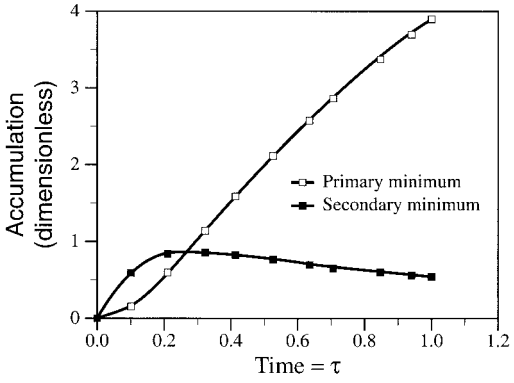

Fig. 9. Primary- and secondary-minimum accumulation for $a\kappa = 220$.

ary condition was applied at R = 5, and 10^3 nodes were specified. Extension to R = 10 for selected cases did not alter the results appreciably.

Results. For an illustrative calculation we used the physical parameters used by Feke and Prabhu (6); i.e., $\zeta_0 = 0.39$, A/kT = 6.0, and a = 2,500 nm, with water as the suspending medium. For this case, in which the Hamaker function was taken to be a constant, the effect of $a\kappa$ on interparticle potential is shown in Fig. 3. At the two lower values of $a\kappa$ the system is electrostatically stabilized against primary minimum coagulation.

Evolution of the pair distribution function is shown in Figs. 4 and 5 for $a\kappa = 200$. It is apparent that particles cluster into a narrow region of separation, and that for $\tau \geq 100$ the distribution is near equilibrium.

In Fig. 6 we show evolution curves for conditions matching our experiments. Because the primary maximum is $O(10^2$ kT), only secondary minimum coagulation is expected.

One is struck by the short times required to effect an appreciable change in the distribution of particles. We see from Fig. 6 that after $0.05 \times 0.15 = 7.5 \times 10^{-3}$ s ($\tau = 0.05$) most of the change has taken place and the distribution is well on its way toward the equilibrium Boltzmann distribution given by the time-independent solution

$$P = \frac{e^{-V(R)} \int_2^R [\exp(V(s))/s^2 G(s)]ds}{\int_2^\infty \exp(V(s))/s^2 G(s)ds}. \qquad [12]$$

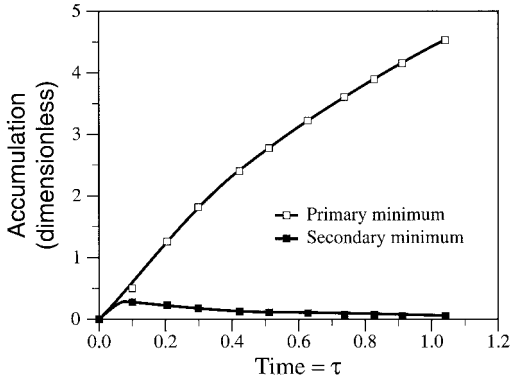

Fig. 10. Primary- and secondary-minimum accumulation for $a\kappa = 230$.

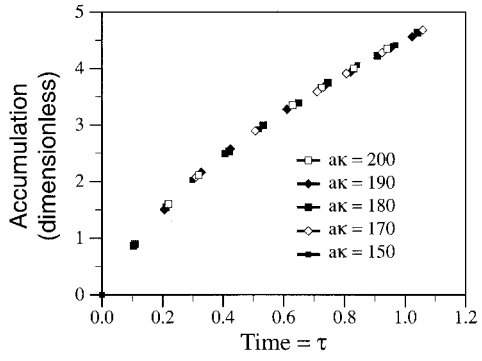

Fig. 11. Total accumulation for $150 \leq a\kappa \leq 200$.

By using Eq. **10**, the accumulation of particles between two shells can be computed. These results must of course be appropriately scaled if one wishes to compare them to experimental data.

An alternate presentation of the above results, that displays the relative importance of flocculation in the primary and secondary minima, is shown in Figs. 7 and 8. The flocculation is essentially all into the secondary minimum for $\tau < 1.0$. However, as the secondary well fills, primary minimum accumulation increases until, for $\tau > 20$, essentially all of the flocculation occurs there.

The results are strongly dependent on ionic strength. Figs. 9 and 10 show that qualitatively different results are obtained at short times when $a\kappa$ is increased to 220 and 230, respectively. The maximum in secondary-minimum population is reminiscent of sequential reaction kinetics, a situation similar to the present phenomenon.

Although the distribution between coagulation in the primary or secondary minimum is strongly affected by ionic strength, the total rate of flocculation is essentially independent of $a\kappa$ over the range studied (see Fig. 11). This is because diffusion-controlled rapid flocculation into the secondary minimum from the far field occurs in each case, independent of the electrostatic field. However, transfer to a primary minimum will occur at a rate affected by the height of the potential barrier and hence by the value of $a\kappa$. One can conveniently collapse the primary minimum accumulation onto a single curve by scaling the accumulation to the value at $\tau = 1.0$. This is shown in Fig. 12.

The time-dependent nature of a coupling between primary and secondary minimum flocculation results in large differences in stability ratios from those calculated from solution of the steady-state diffusion equation,

$$J = -8\pi a^3 \frac{kT}{3\pi\mu a} G(R)\left[\frac{\partial P}{\partial r} + P\frac{\partial V}{\partial R}\right]. \qquad [13]$$

We demonstrate this by plotting in Fig. 13 a stability ratio for primary minimum flocculation scaled on the rapid coagulation

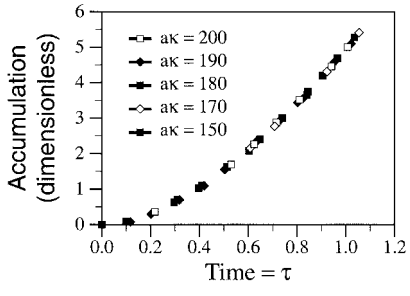

Fig. 12. Primary-minimum accumulation normalized to the value at $\tau = 1.0$.

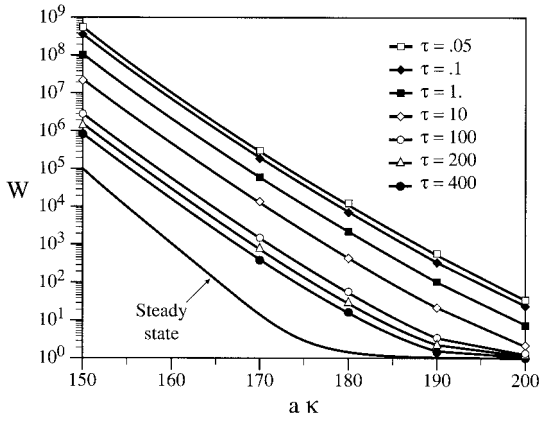

Fig. 13. Time dependence of the stability ratio for primary-minimum flocculation. Results are scaled on the rapid coagulation rate at steady state.

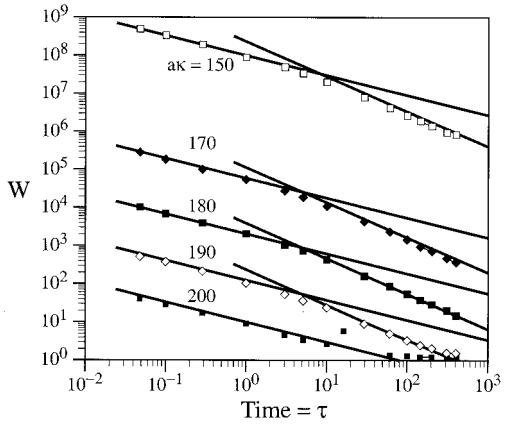

Fig. 15. Time dependence of stability showing two regimes. Results are scaled on the rapid flocculation rate.

rate at steady state. In this case, the stability ratio W is the ratio of the "collision rate" calculated from Eq. **13** to the appropriately scaled integrand of Eq. **10**. For the colloidal parameters used in the model, one dimensionless time unit is equivalent to 35 s. This means that, for the lower ionic strengths, the stability ratio differs from the steady-state value by an order of magnitude after times as large as four hours! The time dependence is shown explicitly for $a\kappa = 150$ in Fig. 14. Note the importance of including the effect of interparticle distance on diffusion, the far-field diffusivity being given by $G(R) = 1$. One of the reasons for the slow approach to steady state is the small separation at which diffusion over the primary maximum takes place. At a separation of 2.01 the hydrodynamic interactions and lubrication forces that act in the near field cause the relative diffusivity of the two spheres to drop to about 2% of the far-field value.

Finally, from Fig. 15 it appears that the flocculation process can be divided into two distinct regions on a logarithmic scale, with the transition occurring at $\tau \cong 5.0$. It is at approximately this time that flocculation into the secondary minimum reaches steady state. At $a\kappa = 200$, steady state is reached before the second regime is entered.

Experiments

Materials. Brownian flocculation experiments were performed with 0.80-μm polystyrene spheres. These were synthesized in nearly monodisperse form (coefficient of variation = 1.7%) using the now-standard method of surfactant-free polymerization (10). Details of preparation and cleaning are described in ref. 7. Flocculation took place in solutions of Fisher ACS-grade sodium chloride dissolved in deionized water. In one series of experiments the NaCl was recrystallized in water before use. It will be seen that this additional purification step had a significant influence on the results.

Particle Counting. The relative abundance of singlets and multiplets was measured with an Elzone Celloscope, a particle counter manufactured by Particle Data, Elmhurst, IL. Aliquots drawn from the flocculating system were added to a 9% solution of NaCl that had been multiply filtered through a 0.22 μm Millipore filter. Electrical resistance was monitored as this solution was drawn through a 15-μm orifice. When a particle (singlet or multiplet) passes through the orifice, the resistance changes as the cube of the effective particle diameter. The concentrated saline solution served two functions: it arrested the flocculation by reducing the particle concentration to a level such that further encounters were negligible, and it "fixed" weakly bonded secondary-minimum multiplets into strongly bonded primary-minimum multiplets.

Procedure. Flocculation was initiated by mixing equal volumes of latex suspension (at volume fractions between 3×10^{-5} and 3×10^{-4}) and electrolyte solution. Mixing was accomplished by pouring the mixture between two containers for 20 s. The temperature was maintained constant at 25 ± 0.1°C. At regular intervals a sample was withdrawn from the quiescent mixture with an Oxford micropipet and added to the saline solution described above. It was found that a concentration of approximately 5×10^5 particles/ml provided enough of a particle flow through the orifice to generate meaningful data, but maintained

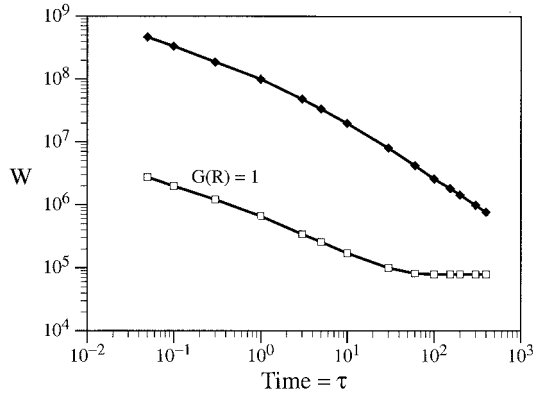

Fig. 14. Time dependence of the stability ratio for $a\kappa = 150$, using $G(R) = 1$ and with the correct value of G(R).

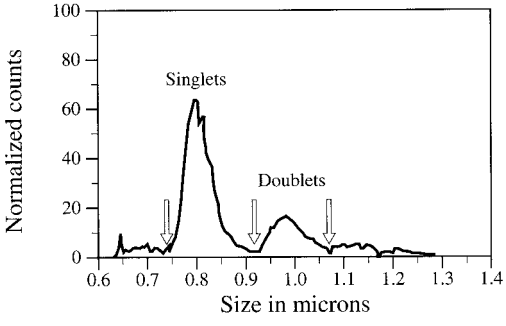

Fig. 16. Sample histogram of a coagulating latex. Arrows show the channels that define singlet and doublet regions.

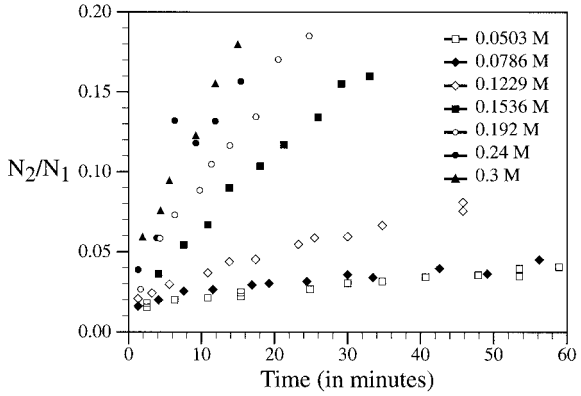

Fig. 17. Ratio of doublets to singlets for a range of ionic strengths.

a probability of less than 1% for a false signal due to simultaneous passage of more than one particle cluster through the orifice.

Naturally, there was concern that the mixing and sampling process might alter weakly bound multiplets. Estimates of shear rates and comparison of data by using a variety of techniques allayed these concerns (7).

Data Analysis. The direct output from the particle counter and associated computer facilities is a histogram of 256 channels that spans particle sizes between approximately 0.6 and 1.6 μm. The numbers of singlets and doublets were compared by adding the number of counts between channels chosen to be their respective limits. A representative histogram is shown in Fig. 16, indicating the discrimination between singlets and doublets (only the first 100 channels are shown). Rate constants were obtained from the slopes of N_2/N_1 as a function of time as time approached zero, because we are interested in comparing the experiments to theory for initial coagulation when the concentration of triplets and higher is negligible.

Results and Discussion

Data showing the doublet/singlet ratio, N_2/N_1 are presented in Fig. 17. In almost all cases, duplicate measurements were made with the particle counter and excellent reproducibility was

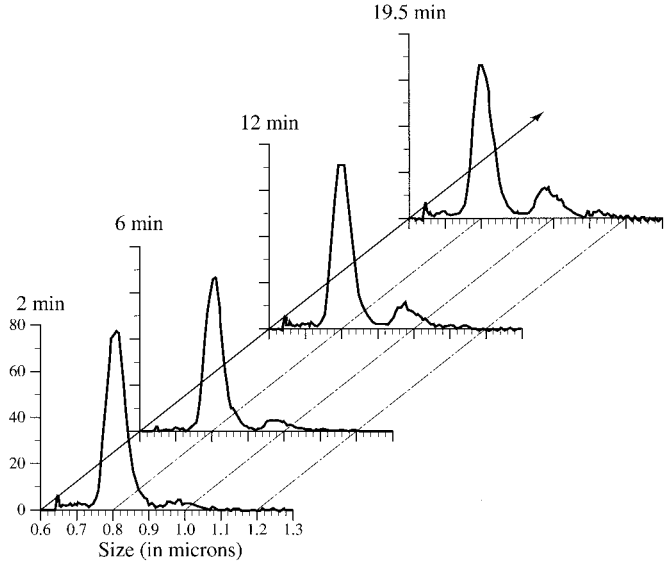

Fig. 18. Brownian flocculation in 0.3 M NaCl. Samples were taken at times indicated above each axis. Particle counts, shown on the vertical axis, are normalized by dividing by the total number of counts and then multiplying by 1,000.

achieved. Scatter increases at the two highest ionic strengths. This increase is due to the necessity to operate at higher dilutions of the latex suspension to maintain sufficiently slow flocculation for sampling and analysis during the period when triplet concentration is negligible. The low concentration gave rise to larger fluctuations in rate of flocculation.

One also notes that the data in Fig. 17 do not have an intercept at the origin. We believe this is not due to the presence of doublets in the initial sample or their formation before sampling occurs. Instead, it is most probably due to noise in the particle counter, which at doublet concentrations lower than 2% is comparable to the signal itself.

It is instructive to look at the evolution of particle size distribution with time, and this is shown in Figs. 18 and 19 for two different electrolyte concentrations. Colloidal parameters for these cases are given in Table 1, where the zeta potential is scaled

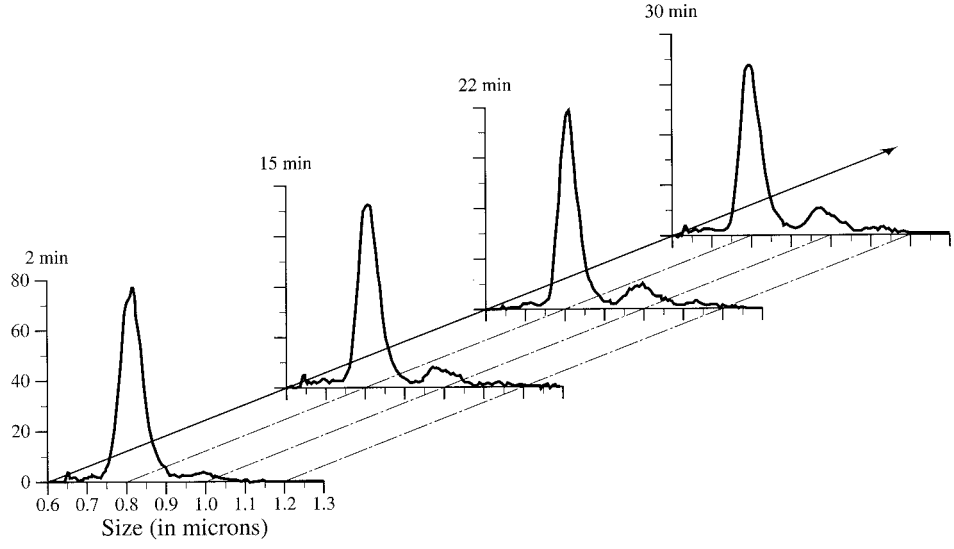

Fig. 19. Brownian flocculation in 0.1613 M NaCl. (See caption for Fig. 18.)

Table 1. Parameters for flocculation experiments shown in Figs. 18 and 19

Ionic strength, molar	aκ	ζ_0	Potential maximum	Potential minimum	Particle volume fraction
0.3000	712	1.22	−10	−26	1.6×10^{-5}
0.1613	522	1.57	129	−13	6.5×10^{-5}

on kT/e and the interparticle potentials on kT. Under conditions of rapid flocculation one can readily distinguish between singlets and doublets.

Stability ratios for the initial stages of flocculation were found from a linear regression of N_2/N_1 as time approached zero. Slopes of these curves were normalized to the rapid-coagulation rate at the highest ionic strengths. Results for two series of experiments are shown in Fig. 20. One notes the significant effect, referred to earlier, of recrystallization of the salt used in the electrolyte. This effect is most likely due to trace amounts of a surface-active agent in the "as received" salt, because a bulk impurity would need to be far greater than that permissible in the grade of salt used. In either case, the transition from slow to rapid flocculation occurs at an electrolyte concentration near 0.1 M.

Once again, we note good reproducibility of results. Repeated measurements on different days were made with the recrystallized electrolyte at concentration 0.06 M $<$ c $<$ 0.11 M and excellent agreement was obtained.

From Fig. 21 one can infer that rapid secondary-minimum flocculation will occur when the secondary-minimum well has a depth of approximately 10 kT.

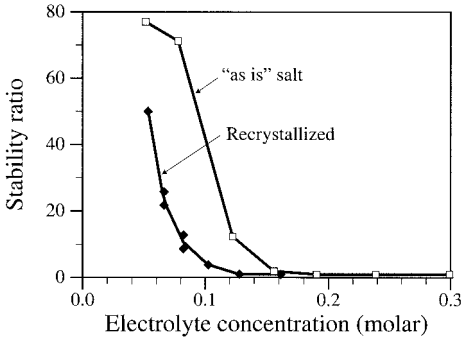

Fig. 20. Comparison of two sets of Brownian experiments with different salt preparation.

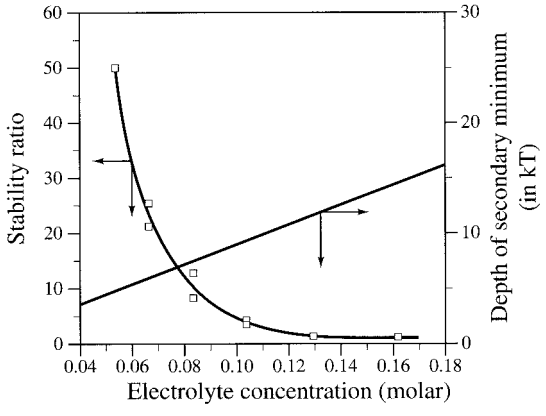

Fig. 21. The experimentally determined stability ratio compared with the potential in the secondary minimum.

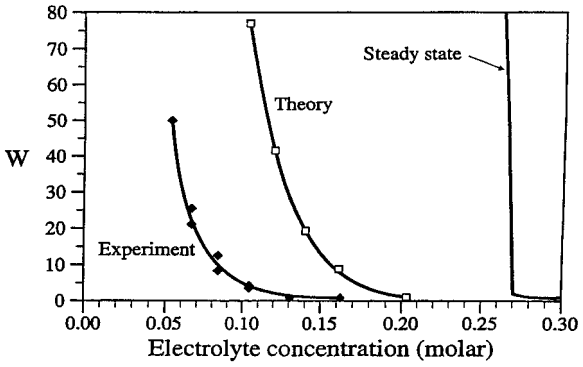

Fig. 22. Comparison of experimental results with theory. The theoretical stability ratio is normalized to 1.0 at an NaCl concentration of 0.2 M.

Finally, in Fig. 22 the experimental results are compared with our theoretical analysis. To put the comparison on an appropriate basis, zeta potential data of Fig. 23 were used, along with an effective Hamaker coefficient (Fig. 2). A relative stability factor was found by computing the integrated flux at a time t = 1 min and normalizing it with the integrated flux for an electrolyte concentration of 0.2 M. The one-minute time interval represents, approximately, the time at which the first experimental samples were taken.

The data marked "experiment" in Fig. 22 represent the recrystallized electrolytes. The "as received" data would be in closer agreement with theory. Nevertheless, the shape of the calculated results corresponds closely with the data, and is a far better representation than predictions based on a steady-state analysis.

One must recognize that all three of the colloidal potentials used in the calculations (attractive, electrostatic repulsive, Born repulsive) are based on continuum models. They have been applied to situations where the interparticle separation can be below one nanometer.

Conclusions

Flocculation of polymer colloids in the presence of a secondary minimum in the interparticle potential curve proceeds far differently from the better-understood process of rapid flocculation into a primary minimum. We have shown that the time dependence due to transfer of particles from one minimum to another can dominate the process. In examples described here, the stability ratio can be an order of magnitude higher than the steady-state result, even after several hours of flocculation. The attenuation in coagulation is caused primarily by hydrodynamic

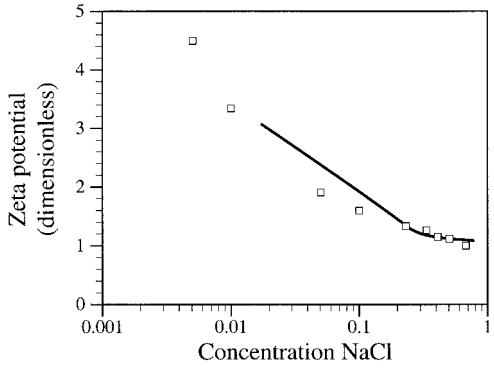

Fig. 23. Zeta potential as a function of NaCl concentration, measured by electrophoresis experiments. Data were approximated with a spline fit.

forces that reduce the diffusion coefficient to a small fraction of its far-field value. When the population of particles in secondary-minimum flocculation reaches a sufficient value, at approximately five dimensionless time units, the rate of flocculation increases as particles are drawn into the primary minimum. This is shown in Fig. 15. (At $a\kappa = 200$, equilibrium is reached before the second regime is entered.) Thus, one concludes that explicit acknowledgment of the coupling between secondary- and primary-minimum flocculation is necessary for satisfactory modeling of Brownian flocculation in the presence of a secondary minimum.

The authors are grateful to Professor Donald Feke for helpful comments on an earlier version of the manuscript. Much of this research was conducted while the authors were associated with Princeton University. Partial support was obtained from the Amoco and Xerox Corporations.

1. von Smoluchowski, M. (1917) *Z. Phys. Chem. (Leipzig)* **92,** 129–168.
2. Russel, W. B., Saville, D. A. & Schowalter, W. R. (1989) *Colloidal Dispersions* (Cambridge Univ. Press, Cambridge, U.K.).
3. van de Ven, T. G. M. & Mason, S. G. (1977) *J. Colloid Interface Sci.* **57,** 505–516.
4. Zeichner, G. R. & Schowalter, W. R. (1977) *AIChE J* **23,** 243–254.
5. Feke, D. L. & Schowalter, W. R. (1983) *J. Fluid Mech.* **133,** 17–35.
6. Feke, D. L. & Prabhu, N. D. (1985) *Langmuir* **1,** 691–696.
7. Eidsath, A. B. (1989) Ph.D. thesis (Princeton Univ., Princeton).
8. Feke, D. L., Prabhu, N. D., Mann, J. A., Jr., & Mann, J. A., III (1984) *J. Phys. Chem.* **88,** 5735–5739.
9. Batchelor, G. K. (1976) *J. Fluid Mech.* **74,** 1–29.
10. Goodwin, J. W., Hearn, J., Ho, C. C. & Ottewill, R. H. (1974) *Colloid Polym. Sci.* **252,** 464–471.